Baseline Determination for Drive Cycle Performance Analysis of Induction Motors

Kourosh Heidarikani
Electric Drives and Machines Institute
Graz University of Technology
Graz, Austria
k.heidarikani@tugraz.at

Pawan Kumar Dhakal
Electric Drives and Machines Institute
Graz University of Technology
Graz, Austria
pawan.dhakal@tugraz.at

Roland Seebacher
Electric Drives and Machines Institute
Graz University of Technology
Graz, Austria
roland.seebacher@tugraz.at

Annette Muetze
Electric Drives and Machines Institute
Graz University of Technology
Graz, Austria
muetze@tugraz.at

***Abstract*—The rise of electric vehicles (EVs) highlights the importance of performance analysis and efficient motor selection, including Induction Motors (IMs). Induction motors provide enhanced efficiency in the flux-weakening region, leading to increased ranges for EVs, and offering robustness and cost-effectiveness compared to permanent magnet synchronous motors (PMSMs). However, it is important to note that IMs experience rotor cage losses at both high and low speeds. Accurate efficiency mapping plays a vital role in facilitating the design of EV motors. Efficiency analysis of dynamic drive cycle operating points is crucial for evaluating vehicle motors. This paper presents a baseline assessment for performance analysis, focusing on enhancing efficiency map accuracy through comprehensive drive cycle analysis using a combination of experiments, analytic modeling, and numerical simulations on a laboratory-scale IM. Analytic and numerical models are created and performance plots are studied for a particular drive cycle covering a wide range of operating points. A dedicated test-rig is set up to examine the transient behavior of the motor during drive cycles, allowing for a thorough analysis of its dynamic performance. The research findings can be generalized to benefit real EV motors.**

***Index Terms*—efficiency maps, induction motors, drive cycles, electric vehicles, traction motors.**

I. Introduction

The increasing demand for electric vehicles (EVs) has highlighted the need to optimize the drive cycle performance of IMs, which are vital components in delivering efficient and reliable propulsion [1]. IMs offer advantages in terms of safety, reliability, cost, and control compared to PMSMs in EVs. In high-speed scenarios, IMs exhibit higher efficiency by reducing the current in the flux-weakening region, while PMSMs require the injection of negative current. However, in low-speed or high-torque conditions, IMs may experience increased losses due to their rotor cage losses and the strong dependency of the rotor resistance on the temperature can affect the control. Control of IMs is generally easier than control of PMSMs, and in the event of inverter faults, they naturally de-excite, providing increased reliability and safety compared to PMSMs. Additionally, the high cost of magnets in PMSMs stimulates designers to favor the selection of IMs to reduce vehicle expenses [2], [3]. Analyzing the IM performance in EVs across diverse drive cycles is vital for optimizing their design, control strategies, and efficiency. Precise assessment of efficiency under varying conditions is crucial for reducing emissions and extending vehicle ranges [4], [5].

Efficiency maps are essential for predicting motor performance and optimizing energy consumption in electric vehicles. Ensuring accuracy at transient operating points is crucial for reliable efficiency maps, aiding system design and motor selection for optimal IM efficiency [6], [7]. While model-derived efficiency maps offer advantages like virtual testing and deeper insights, challenges related to model accuracy and transient effects must be addressed [8]–[10].

This research is dedicated to addressing the challenges related to efficiency predictions within drive cycles and evaluating the associated confidence levels. The primary focus is on eventually enhancing the accuracy of performance maps by conducting a detailed analysis of IM efficiency at operating points derived from drive cycles. These cycles encompass various operating points with different vehicle speeds and torques, which are determined using a quasi-static longitudinal vehicle model (QSS) [11], [12]. The QSS model provides a simplified representation of the vehicle's mechanical behavior. The WLTP (Worldwide Harmonized Light Vehicle Test Procedure) class 3 drive cycle is selected for evaluation, as it effectively covers a range of demanding operating points.

To contribute to a better understanding of the accuracy of the use of performance maps, this study conducts a comprehensive analysis integrating experimental investigations, analytic modeling, and numerical simulations. In this first step, time-stepping analyses are used. A crucial step involves using down-scaled drive cycles for two different range vehicle QSS models, which can be utilized in both the models and experiments conducted with test case motors in the laboratory. Experimental validation through tests on motor prototypes is crucial for determining accuracy of the different approaches and also generalise the results for IMs in the EV

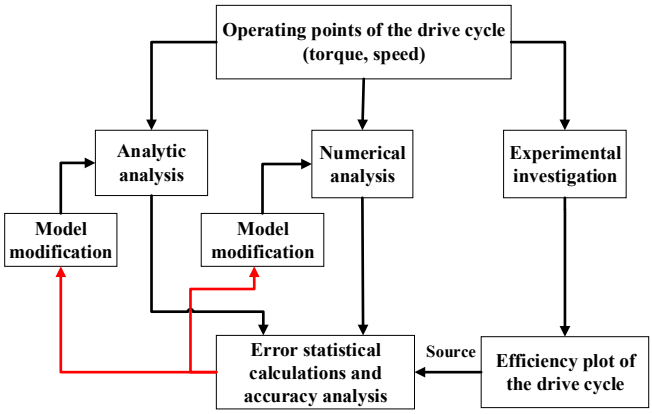

Fig. 1. Workflow of the study.

range. By comparing measured and predicted efficiencies of the time-stepping analyses, the confidence levels associated with the maps can be later evaluated. This research also examines the temperature-dependent characteristics of the selected parameters. Here, we focus on the winding losses, and on friction losses in the analytic model, and solely on winding losses in the numerical model. This approach aims to improve the understanding of the most important factors affecting the accuracy of the analysis. The workflow of this study is presented in Fig. 1. Section 2 presents the baseline employed in this research, including the test case studies, experimental setup, analytic modeling approach, and numerical simulation techniques. Section 3 presents the results obtained from the analysis, showcasing the comparisons between the models' efficiencies and discussing the reason of the differences and accuracy analysis. Finally, Section 4 concludes the paper by summarizing the findings.

II. Baseline Determination

This section identifies a baseline of this research. The test case studies will be presented and also the procedure of each type of analysis, analytic, numerical, and experimental setup, will be explained.

A. Test case studies

In this study, for the investigation of the efficiency prediction, a mid-range (BMW i3) and a small-range (Smart EQ) passenger car were selected to use their specifications in the QSS model to obtain the required torque for the drive cycle. To experimentally study the operating points of the driving scenarios, one IM is available in the laboratory. The vehicles and the lab motor's specifications are listed in Table I. By considering the motor's specification, the torque-speed profiles of the motors used in these cars for the WLTP class 3 drive cycle as shown in Fig. 2 are obtained. Due to the lower rating of the laboratory motor compared to the motor in the selected cars, the operating points obtained for the vehicles' motors needed to be adjusted for compatibility with the laboratory setup. To achieve this, a mathematical method combined with the motors' parameters is used [14], and a down-scaling process was applied to obtain

TABLE I
Vehicle Motor and Laboratory Motor Specifications [16], [17]

Vehicle Motor Specifications		
Parameters	**Values**	
	BMW i3	**Smart EQ**
Machine Type	PMSM	PMSM
Maximum Torque	250 Nm	161 Nm
Maximum Power	125 kW	61 kW
Base Speed	4800 rpm	3581 rpm
Maximum Speed	11400 rpm	11475 rpm
Lab Motor Specifications		
Parameters	**Values**	
Max. Power	4.4 kW	
Max. Torque	30.5 Nm	
Rated Speed	1430 rpm	
Maximum Speed	2850 rpm	

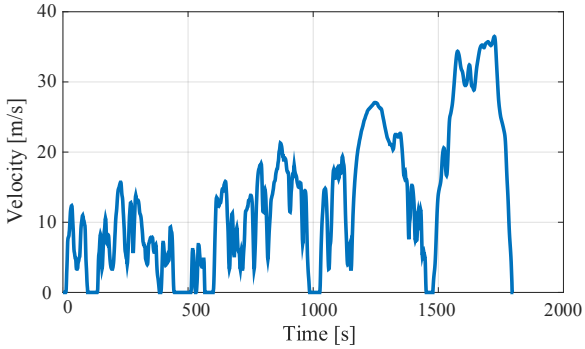

Fig. 2. WLTP class 3 drive cycle.

the operating points within the range of the laboratory motor. The research utilized the operating points obtained from this process to conduct the analysis and experimentation. The visual representation of the operating points during the WLTP class 3 drive cycle for two actual vehicle motors and the test case motor utilized in this study is shown in Fig. 3. These operating points were obtained from the quasi-static model of the BMW i3 and Smart EQ. Subsequently, they were down-scaled to align with the specifications of the laboratory's IM [15]. Note that this downscaling may lead to a low utilization of the motor.

B. Analytic analysis

The analytic analysis was conducted using MATLAB/Simulink [18], involving the development of a precise model for the IM and its control system. The motor parameters were obtained through experimental tests. Notably, the model accounted for friction losses and iron losses, taking into consideration the specific characteristics observed during the experiments. Fig. 4 presents the control system of the IM using the Rotor Oriented Flux Control (RFOC) that can support transient behaviour required by the drive cycles. This simulation considered a speed filter and also an encoder model to align to the real experiment. The temperature coefficient obtained from the experiment is taken into account for both the rotor and the stator resistance in the model. Additionally, considering the temperature effect

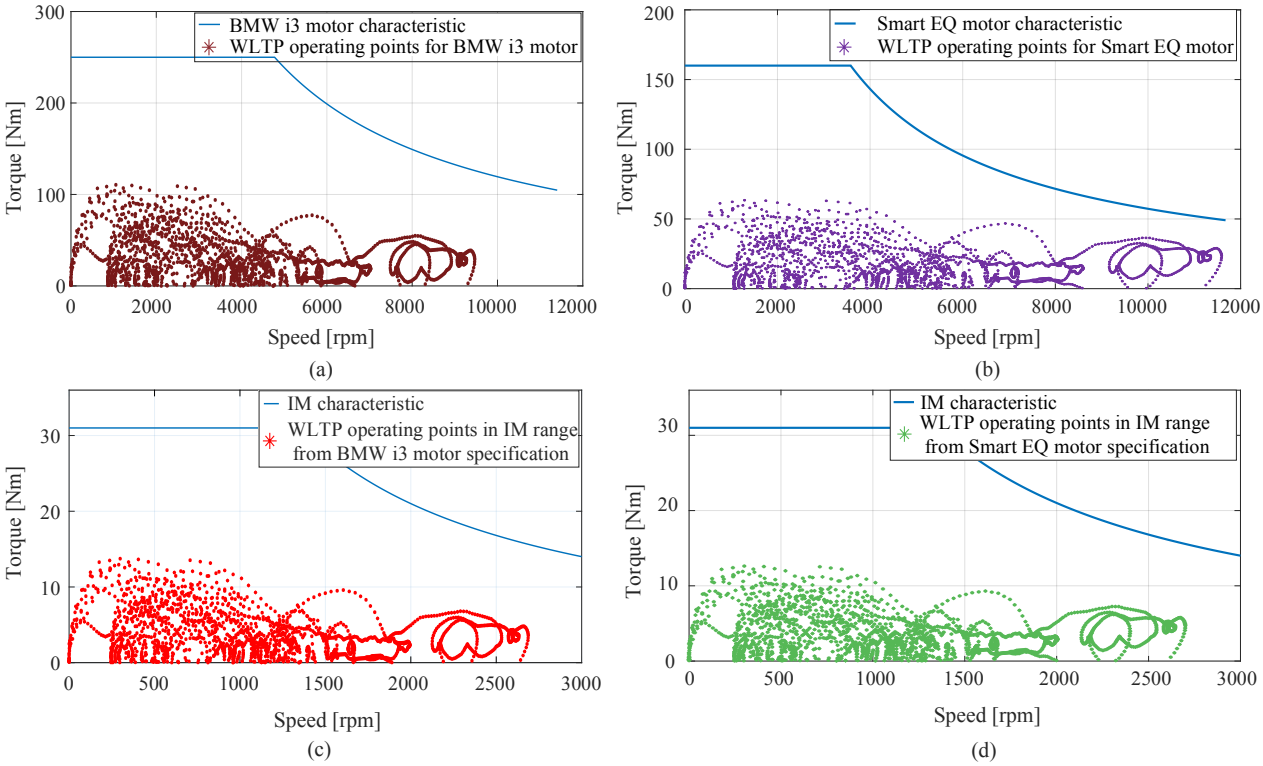

Fig. 3. Torque-speed operating points for the WLTP drive cycle: (a) BMW i3, (b) Smart EQ, (c) down-scaled for BMW i3 to the laboratory IM's range, (d) down-scaled for Smart EQ to the laboratory IM's range.

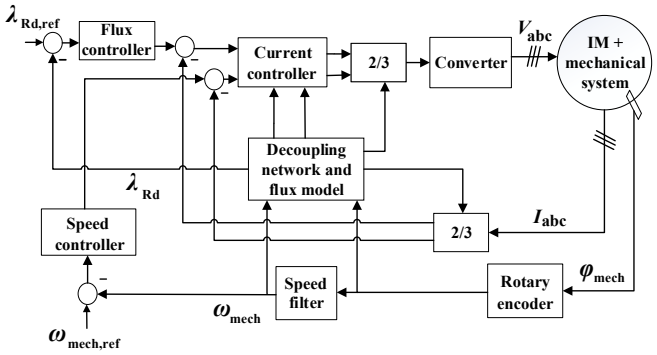

Fig. 4. Analytic motor RFOC block diagram.

on the bearing's oil, the frictional torque coefficient is also incorporated into the model [19]. The efficiency is calculated according to (1), where P_{out} is the output power of the motor, P_{Cu} is the total stator and rotor resistance losses, P_{Fe} is the iron losses, and P_{Fric} denotes the friction losses. To simplify the analysis, only the operating points in the motoring mode of the motor torque-speed profile are exclusively considered, with the potential to extend this approach to the generator mode as well.

$$\eta = \frac{P_{\text{out}}}{P_{\text{out}} + P_{\text{Cu}} + P_{\text{Fe}} + P_{\text{Fric}}} \times 100\% \qquad (1)$$

C. Numerical analysis

Numerical simulations were performed to analyze the efficiency of the motor by Finite Element Analysis (FEA). The simulations were carried out using the JMAG® software [20], which allowed for accurate representation and analysis of the motor's behavior in 2D and 3D environments. In this research, a 2D model was employed to capture the electromagnetic characteristics of the motors under different operating points within the drive cycles. In this approach, we take into account the temperature-dependent characteristics of the stator and the rotor cage resistances. It is important to emphasize that a comprehensive thermal analysis, encompassing temperature considerations for various losses, will be carried out separately in the future. Furthermore, the mesh size can strongly influence the output of the simulation. The finer the mesh, the more precise the result. The half 2D FEA model of the IM in JMAG® is shown in Fig. 5. In this model, the iron losses of the stator material and also the exact winding configuration of the stator are considered. The rotor end ring leakage inductance and the resistance of the motor was taken into account. A basic PWM control system has been employed to create an efficiency plot from this model. Due to this model's capabilities, it is imperative to emphasize that this approach does not include RFOC and follows straightforward operation. JMAG® is equipped to produce a motor response table for each torque-speed operating point in a steady-state condition. This table serves as a grid, and the accuracy of the motor's performance is closely linked to the granularity of this grid.

D. Experimental investigation

The laboratory tests for the IM have been successfully completed. The control system, as illustrated in Fig. 4, was

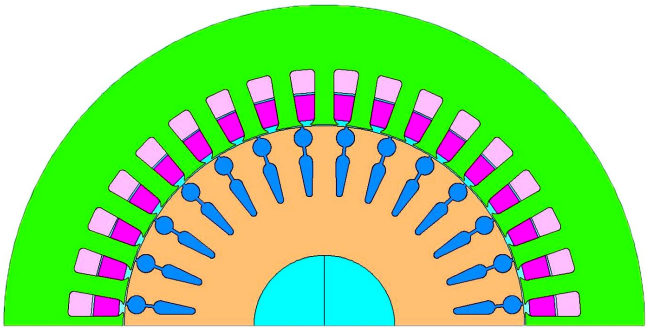

Fig. 5. A 2D FEA model of IM in JMAG® designer.

employed in the laboratory setup. To enhance the model accuracy by considering temperature effects, a significant number of temperature sensors are available.

During these tests, various parameters were recorded for analysis. This included measurements of the stator voltage and current, as well as the output torque and speed of the motor, throughout the drive cycles. The laboratory setup also included a load machine, which is a Permanent Magnet Synchronous Motor (PMSM). It is important to note that the PMSM in this setup is torque-controlled, and a torque sensor has been installed on the shaft between the two motors to monitor and measure torque accurately. This data collection process allowed for the calculation of energy conversion within the motor and the creation of precise efficiency plots. These results can be used for analysis and comparison with the models developed. Furthermore, in all experimental tests, the motor temperature was raised to 30 °C using a heater before commencing the tests, such heating is needed because of the down-scaling that led to low thermal utilisation.

III. Result and Discussion

Both numerical and analytic analyses were performed at a specific temperature (30 °C) to evaluate the efficiency of the IMs within the operating points of the selected drive cycle. The analysis focused on the WLTP class 3 drive cycle, chosen for its comprehensive coverage of speed and torque ranges relevant to various driving conditions, including rural and inter-city scenarios.

In Fig. 6, efficiency plots are presented, encompassing various methods, including numerical and analytic simulations, alongside experimental tests. These plots correspond to operational conditions derived from both BMW i3 and Smart EQ motors, and they were obtained from energy conversion during the drive cycle for each operating point. In most operating points, there is a noticeable similarity among the graphs, indicating a strong concurrence between the drive cycle simulation methods employed in both models and the results from experimental tests. This underscores the effectiveness of the baseline determination. However, as depicted in Fig. 6, substantial differences are evident, highlighting the influence of factors such as the temperature effect on rotor losses, mechanical friction, parameter uncertainty, and variations in the control methods of the inverter and control system.

A. Accuracy analysis

For assessing the accuracy and error of the models in comparison to the experimental results, two statistical methods are employed. The Root Mean Square Error (RMSE) serves as a measure to quantify the average magnitude of discrepancies between two sets of data. It proves particularly valuable when evaluating the precision of a model's predictions relative to the experimental data. RMSE can be computed according to (2), where N, m_{i}, and s_{i} denote the number of data points, efficiency for each points from the models (analytic and numerical) and efficiency from experimental test [21].

$$\mathrm{RMSE} = \sqrt{\frac{1}{N}\sum_{i=1}^{N}|m_{\mathrm{i}} - s_{\mathrm{i}}|^2} \tag{2}$$

The second method involves the use of the Correlation Coefficient, which assesses the strength and direction of a linear relationship between the model's predictions and experimental data. The correlation coefficient is computed using (3), where σ_{X} and σ_{Y} are the standard deviations of model and experimental result respectively, and cov(X, Y) is their covariance. The correlation coefficient ranges from -1 to 1. A high positive correlation signifies similar patterns, while a low/near-zero correlation suggests a weaker connection, with the sign indicating its direction [21].

$$\text{Correlation Coefficient}(\mathrm{r}) = \frac{\mathrm{cov}(\mathrm{X},\mathrm{Y})}{\sigma_{\mathrm{X}} \cdot \sigma_{\mathrm{Y}}} \tag{3}$$

These two methods were implemented, and the results are presented in Table II. The correlation coefficients in both models underscore the similarity in efficiency patterns compared to experimental data. However, it is noteworthy that the table results indicate a higher efficiency error in the numerical simulation. This difference can be attributed to several contributing factors. First: the control system employed in the numerical simulation differs significantly from the one used in the experimental and analytic approaches. Additionally, the numerical simulation neglects the consideration of a fixed flux and initiates the efficiency map from zero current instead of commencing from the magnetization current, which serves as a predefined reference point within the control system in Fig. 4. Furthermore, in the numerical simulation conducted within JMAG®, linear friction losses that increase linearly with speed are considered, as opposed to employing a non-linear equation [22]. Moreover, as the drive cycle progresses, the motor temperature rises, impacting the copper and the cage losses as well as friction

TABLE II
Efficiency Error Analysis in Analytic and Numerical Simulations

	Smart EQ		**BMW i3**	
	RMSE	**r**	**RMSE**	**r**
Analytic	2.78	0.9959	3.12	0.9952
Numerical	8.91	0.9708	9.83	0.9650

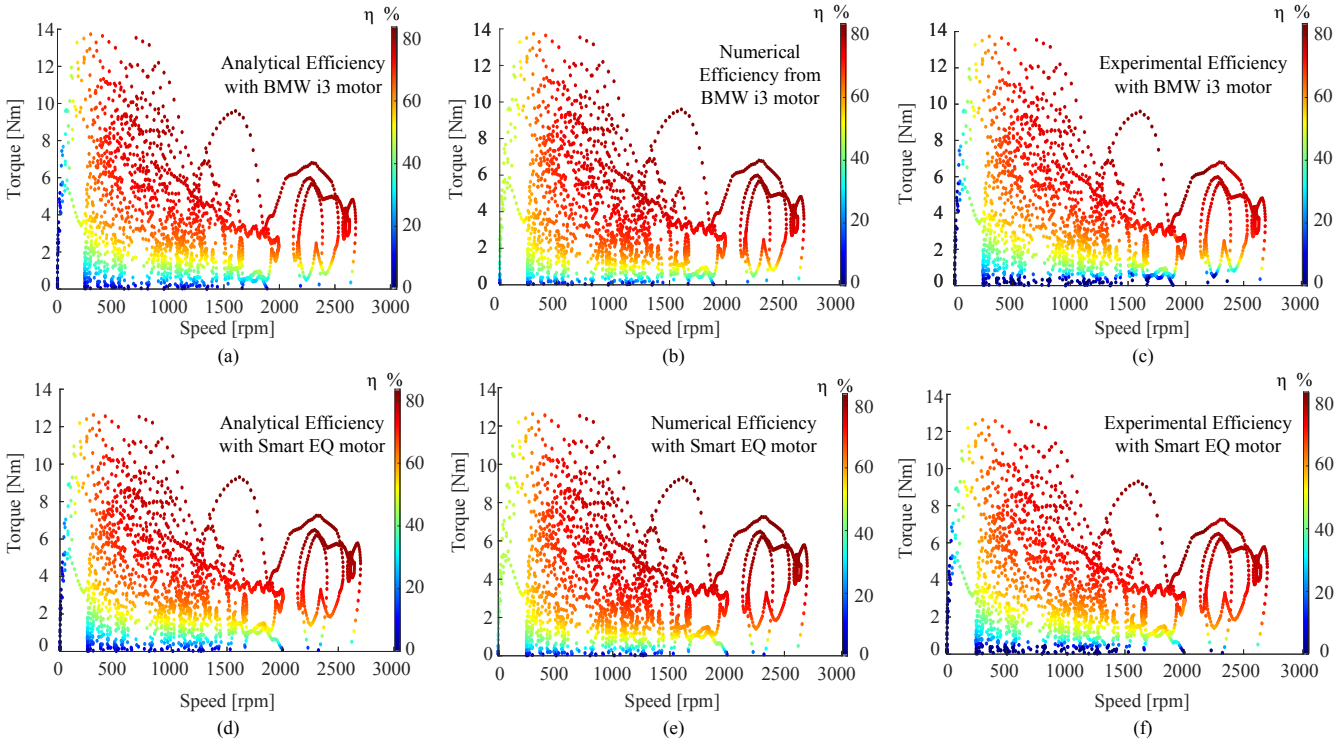

Fig. 6. Efficiency plots of IM: (a) analytic result with operating points obtained from BMW i3, (b) numerical result with operating points obtained from BMW i3, (c) experimental result with operating points obtained from BMW i3, (d) analytic result with operating points obtained from Smart EQ, (e) numerical result with operating points obtained from Smart EQ, (f) experimental result with operating points obtained from Smart EQ.

losses. However, in the JMAG® simulation, only fixed resistances are considered for both stator and rotor resistances, which could potentially introduce deviations in both overall losses and efficiency.

Despite the analytic model showing a lower error compared to the numerical model, it still exhibits significant inaccuracies, potentially owing to uncertainties in the model. These uncertainties may arise from the not accounting for the impact of temperature on the parameters, as well as potential factors like iron loss, friction loss, and the skin effect.

B. Sensitivity analysis

To gain a deeper insight into the factors affecting the model accuracy, such as temperature, analyses were performed to evaluate how temperature influences the precision of the model's efficiency predictions. Modifications were implemented for the resistance values in both analytic and numerical simulations, taking into account temperature variations in both the stator and the rotor windings. The analyses were guided by temperatures observed throughout the drive cycle experiments, where the temperature increased from 30 °C to 60 °C throughout the cycle. Specific attention was given to the maximum temperature of 60 °C occurring within the stator winding and the average temperature of 40 °C within the motor winding across drive cycles. Additionally, changes to the coefficient controlling the temperature dependency of friction losses were exclusively made in the analytic simulation. Following these modifications, two simulation runs

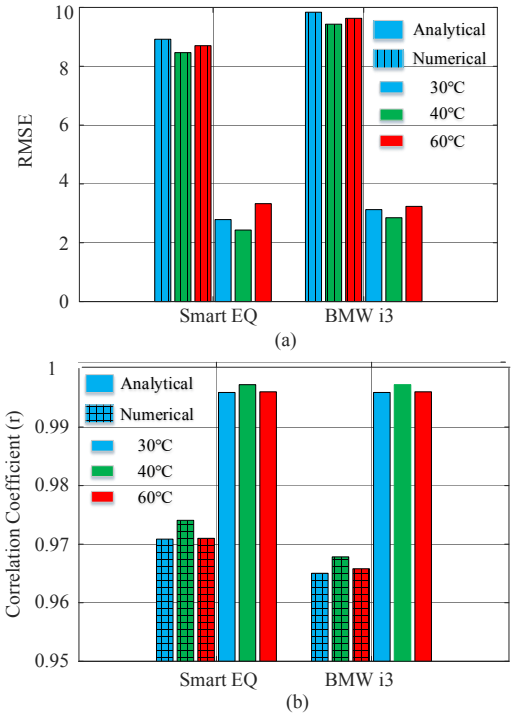

Fig. 7. Accuracy analysis of efficiency values of operating points in different winding temperatures. (a) RMSE, (b) Correlation Coefficient.

were conducted, each incorporating the adjusted resistance values, and accuracy analyses were carried out on the results.

Fig. 7 illustrates the Root Mean Square Error (RMSE) and the correlation coefficient (r) comparing both numerical and

analytic results to the experimental data. This comparison is conducted across operating points for both the Smart EQ and the BMW i3 vehicles under different temperature conditions.

As seen in Fig. 7, the RMSE of the efficiency values at $40\,^{\circ}\mathrm{C}$ decreased in all analyses, indicating closer alignment with the experimental values for both smart EQ and BMW i3 operating points. Correlation coefficients have also improved at this average temperature. However, at the maximum temperature of $60\,^{\circ}\mathrm{C}$, errors show minimal change, indicating that the revision of winding losses to this temperature may not be the key to reduce the errors.

IV. Conclusion

This study investigates dynamic performance analyses of IMs concerning their applicability in specific electric vehicles (EVs) due to their cost-effectiveness and simplified control compared to PMSMs. Analytic and numerical models were created to analyze the WLTP class 3 drive cycle, incorporating down-scaled torque-speed points within the laboratory's IM range, originating from two different vehicles. The performances of different operating points were studied both analytically and numerically at specific temperature, and experimental tests were also conducted.

Performance plots derived from simulation analysis display notable discrepancies when contrasted with experimental results, primarily owing to the impact of temperature on the rotor and the stator winding losses, mechanical friction, and variations within the control systems. Accuracy analysis was performed using root mean square error and correlation coefficient methods to measure the errors and the similarity between simulations and experimental results. The numerical model exhibited more errors due to limitations in replicating the control system accurately, as well as inaccuracies in the friction losses equation within the software. To better understand the effect of temperature on the model accuracy, the resistances of the stator and rotor windings were adjusted in both the analytic and numerical models, considering their temperature dependency. Additionally, in the analytic model, the temperature-dependent coefficient of friction was modified. The results showed that at the motor's average temperature, errors decreased, and the correlation coefficient increased. This implies that by modifying temperature-related parameters, errors can be minimized.

Overall, this study provides valuable insights into the precision and reliability of analytic and numerical methods for depicting motor efficiency across diverse operating points.

Acknowledgment

This work is supported by the joint DFG/FWF Collaborative Research Centre CREATOR (CRC – TRR361/F90) at TU Darmstadt, TU Graz and JKU Linz.

References

[1] A. K. Singh, A. Dalal, and P. Kumar, "Analysis of induction motor for electric vehicle application based on drive cycle analysis," in 2014 IEEE International Conference on Power Electronics, Drives and Energy Systems (PEDES), Mumbai: IEEE, Dec. 2014, pp. 1–6.

[2] J. Su, R. Gao, and I. Husain, "Model Predictive Control Based Field-Weakening Strategy for Traction EV Used Induction Motor," IEEE Transactions on Industry Applications, vol. 54, no. 3, pp. 2295–2305, May 2018.

[3] G. Pellegrino, A. Vagati, B. Boazzo, and P. Guglielmi, "Comparison of Induction and PM Synchronous Motor Drives for EV Application Including Design Examples," IEEE Transactions on Industry Applications, vol. 48, no. 6, pp. 2322–2332, Nov. 2012.

[4] "A performance study of a high-torque induction motor designed for light electric vehicles applications — SpringerLink." https://link.springer.com/article/10.1007/s00202-021-01331-4 (accessed Jun. 09, 2023).

[5] Y. Shi and R. D. Lorenz, "Induction machine design for dynamic loss minimization along driving cycles for traction applications," in 2017 IEEE Energy Conversion Congress and Exposition (ECCE), Oct. 2017, pp. 278–285.

[6] L. di Leonardo, M. Popescu, G. Fabri, and M. Tursini, "Performance Evaluation of an Induction Motor Drive for Traction Application," in IECON 2019 - 45th Annual Conference of the IEEE Industrial Electronics Society, Lisbon, Portugal: IEEE, Oct. 2019, pp. 4360–4365.

[7] B. Dianati, S. Kahourzade, and A. Mahmoudi, "Optimization of Axial-Flux Induction Motors for the Application of Electric Vehicles Considering Driving Cycles," IEEE Transactions on Energy Conversion, vol. 35, no. 3, pp. 1522–1533, Sep. 2020.

[8] S. Pastellides, S. Gerber, R.-J. Wang, and M. Kamper, 'Evaluation of Drive Cycle-Based Traction Motor Design Strategies Using Gradient Optimisation', Energies, vol. 15, no. 3, p. 1095, Feb. 2022.

[9] M. Salameh, I. P. Brown, and M. Krishnamurthy, 'Driving Cycle Analysis Methods Using Data Clustering for Machine Design Optimization', in 2019 IEEE Transportation Electrification Conference and Expo (ITEC), Detroit, MI, USA, Jun. 2019, pp. 1–6.

[10] S. Sridharan and P. T. Krein, "Induction motor drive design for traction application based on drive-cycle energy minimization," in 2014 IEEE Applied Power Electronics Conference and Exposition - APEC 2014, Mar. 2014, pp. 1517–1521.

[11] L. Guzzella and A. Amstutz, 'The QSS Toolbox Manual'. Jun. 2005. Available: https://idsc.ethz.ch/research-guzzella-onder/downloads.html.

[12] C. Paar and A. Muetze, 'Influence of Dry Clutch and ICE Transmission Integration on the Thermal Load of a PM-Based Integrated Starter-Generator', IEEE Trans. Transp. Electrification, vol. 3, no. 3, pp. 716–723, Sep. 2017.

[13] S. Kamguia Simeu and N. Kim, 'Standard Driving Cycles Comparison (IEA) & Impacts on the Ownership Cost', in WCX World Congress Experience, Apr. 2018.

[14] M. D. Petersheim and S. N. Brennan, 'Scaling of hybrid-electric vehicle powertrain components for Hardware-in-the-loop simulation', Mechatronics, vol. 19, no. 7, pp. 1078–1090, Oct. 2009.

[15] P.K. Dhakal, K. Heidarikani, and A. Muetze, 'Down-scaling of drive cycles for experimental drive cycle analyses', in 12th International Conference on Power Electronics, Machines and Drives (PEMD 2023), Brussels, Belgium, Oct. 2023.

[16] 'Technical Data BMW i3 ', https://www.press.bmwgroup.com/global /article/detail/T0148284EN/the-bmw-i3?language=en, (accessed Sep. 1, 2023).

[17] "Smart EQ fortwo coupe," EV Database. https://ev-database.org/car/1230/Smart-EQ-fortwo-coupe (accessed Sep. 1, 2023).

[18] "MATLAB." Accessed: Sep. 18, 2023. [Online]. Available: https://www.mathworks.com/products/matlab.html

[19] B. Maru and P. A. Zotos, "Anti-friction bearing temperature rise for NEMA frame motors," IEEE Transactions on Industry Applications, vol. 25, no. 5, pp. 883–888, Sep. 1989, doi: 10.1109/28.41253.

[20] "Simulation Technology for Electromechanical Design: JMAG." https://www.jmag-international.com/ (accessed Sep. 12, 2023).

[21] D. C. Montgomery, E. A. Peck, and G. G. Vining, Introduction to Linear Regression Analysis. John Wiley & Sons, 2021.

[22] B. SKF, "The SKF model for calculating the frictional moment," SKF, 2014.